Oxidation state and lattice expansion of CeO_{2-x} nanoparticles as a function of particle size

Lijun Wu, H. J. Wiesmann, A. R. Moodenbaugh, R. F. Klie, Yimei Zhu, D. O. Welch, and M. Suenaga
Materials Science Department, Brookhaven National Laboratory, Upton, New York 11973, USA
(Received 7 November 2003; published 24 March 2004)

Cerium oxide nanoparticles CeO_{2-x} (~3–20 nm in diameter) made by a vapor phase condensation method, have been studied by several methods of transmission electron microscopy (TEM): electron energy loss spectroscopy (EELS), high resolution imaging, and electron diffraction. The white-line ratios M_5/M_4 of the EELS spectra were used to determine the relative amounts of cerium ions Ce^{3+} and Ce^{4+} as a function of particle size. The fraction of Ce^{3+} ions in the particles rapidly increased with decreasing particle size below ~15 nm in diameter. The particles were completely reduced to $CeO_{1.5}$ at the diameter of <~3 nm. This reduced cerium oxide has a fluorite structure which is the same as that of bulk CeO_2. Also, EELS spectra taken from the edge and center of the particle indicated that for larger particles the valence reduction of cerium ions occurs mainly at the surface, forming a $CeO_{1.5}$ layer and leaving the core as essentially CeO_2. A micromechanical model based on linear elasticity was used to explain the lattice expansion of the CeO_{2-x} nanoparticles. Comparing our results with previously published works indicates that the amount of $CeO_{1.5}$ in CeO_{2-x} nanoparticles is a strong function of the particular synthesis methods used to make these particles.

DOI: 10.1103/PhysRevB.69.125415 PACS number(s): 73.22.−f, 68.37.Lp, 79.20.Uv, 61.46.+w

I. INTRODUCTION

Ceria has been widely studied since it is easily reduced or oxidized and this property is very important for its applications, such as catalysts in vehicle emissions-control systems[1] and electrolyte materials in solid oxide fuel cells.[2] For applications as a catalyst, fine particles of ceria are fabricated to increase surface area in order to enhance the catalytic efficiency. In order to understand the properties of fine ceria particles, a large number of studies have been carried out on catalytic,[3,4] electronic,[5] lattice vibrational,[6,7] and structural[8–12] properties as well as on various synthesis methods[12–14] for ultrafine ceria particles. However, in spite of the practical importance of and the scientific interests in these nanosized particles, no systematic study of properties as a function of size had been made until a series of articles by Tsunekawa *et al.* were published.[5,8,10,13] Using so-called monodisperse nanoparticles of ceria, which were made by a hydrothermal process,[13] with different dimensions, they observed that the lattice parameters, as determined by electron diffraction, of the nanoparticles increased with decreasing particle size.[8] Based on the analysis of the particle size dependence of the lattice parameter, they suggested that this expansion was due to the loss of oxygen from the surface region of CeO_2 particles. Also, they claimed that the particle of CeO_{2-x} would be fully reduced to $CeO_{1.5}$ when the size of the particles became 1.5 nm and its structure would be the C-type cubic sesquioxide Ce_2O_3. This structure of Ce_2O_3 has not been observed in bulk ceria although it is a common structure in some other lanthanide oxides. The structure of bulk Ce_2O_3 is an *A*-type hexagonal sesquioxide.[15] Furthermore, using an x-ray photoelectron spectroscopy technique (XPS) they confirmed the existence of Ce^{3+} ions in the small particles and the increased ratio of Ce^{3+}/Ce^{4+} with decreasing size.[5] In addition, they claimed in this article that these Ce^{3+} ions are in fact primarily in the surface region of the particles in agreement with their earlier suggestion. More recently, in their theoretical study, they attributed the observed lattice expansion to the decrease of the electrostatic force caused by the valence reduction of Ce ions in the ceria.[10]

Recently, the lattice expansion as a function of particle size has also been measured by x-ray diffraction measurements for monodispersed particles which were prepared by a room-temperature precipitation method.[12] Interestingly, as discussed in detail below, Zhang *et al.*[12] found much smaller expansions of the lattice than those found in the study by Tsunekawa *et al.*[5] For example, Zhang *et al.* reported a lattice expansion of ~0.3% for ~7 nm ceria particles while Tsunekawa *et al.*[5] reported ~0.8% for similar-sized particles. Thus, further investigation of the electronic and structural properties of nanocrystalline CeO_{2-x} as a function of the particle size is of interest.

In this article, we report the results of an investigation of the valence of Ce ions in CeO_{2-x} nanoparticles as a function of their size using electron microscopy techniques: electron energy loss spectroscopy (EELS), high resolution imaging, and electron diffraction. The particles were prepared by vapor phase condensation of CeO_2 in an inert gas atmosphere. The advantage of using EELS in a high resolution transmission electron microscope is that a single nanoparticle can be examined, and the size and crystal structure of that individual particle may be determined simultaneously. Other techniques with larger probe sizes, such as XPS, require a large assembly of particles with unavoidable variations in size, even when the new synthesis techniques have narrowed the size distribution[12,13] of the so-called monodisperse nanoparticles. In addition, with the improved spatial resolution of EELS, it is possible to examine directly the local variations, such as bulk vs surface regions, in the Ce^{3+}/Ce^{4+} ratios within a given particle.

II. EXPERIMENTAL PROCEDURE

The cerium oxide nanoparticles were synthesized using the technique of thermal evaporation of CeO_2 in a helium

atmosphere. A vacuum chamber was initially pumped to a base pressure of about 10^{-5} Torr using a turbomolecular pump. Helium was next admitted into the chamber until the desired pressure, ~1–100 Torr, was attained. The pressure was measured with a diaphragm capacitance manometer gauge. Bulk cerium oxide pieces were next thermally evaporated from a tungsten crucible. The time-temperature profile of the crucible was controlled using a programmable power supply. The crucible temperature during evaporation was about 2000 °C as measured with an optical pyrometer. Copper TEM specimen grids, which were coated with lacy carbon, were placed in the vacuum chamber at strategic locations near the tungsten crucible. The ceria nanoparticles were collected on the lacy carbon coated side of the grids during the course of evaporation. After the evaporation was completed the grids were removed from the vacuum chamber for TEM analysis. It was found that the particle size increases with increasing helium pressure. A series of ceria nanoparticles with particle size from ~3 to ~20 nm in diameter were obtained.

The TEM experiments were carried out in a 300 KV JEOL-3000FEG transmission electron microscope equipped with a Gatan imaging filter (GIF), an annular dark-field detector, and an image-plate recording system. The microscope can be operated in either TEM or scanning transmission electron microscope (STEM) mode. In general, the TEM mode was used to obtain high resolution images and diffraction patterns for lattice parameter measurements, while STEM mode was employed to obtain EELS spectra for individual particles. The probe size in STEM was approximately 0.13 nm, the convergent angle was 11 mrad, and the collection angle was 24 mrad. Because electron beam irradiation for extended periods risks damage,[16] with a resulting change of the valence of Ce ions from Ce^{4+} to Ce^{3+} due to the loss of oxygen, we used a short EELS acquisition time of 2 s. Changes in the spectra due to the exposure started to become noticeable when the acquisition time was extended to 30 s or more. In order to limit exposure of an individual particle, only one spectrum per particle was taken except when the EELS data were taken across the diameter of the particles to investigate local variations in the valence of the ions.

Electron energy loss spectra and x-ray absorption spectra (XAS) or XPS in the *M*-edge region of rare-earth elements carry information on the initial state $4f$ occupancy. The spectra are characterized by sharp white lines of $3d_{3/2} \rightarrow 4f_{5/2}\,(M_4)$ and $3d_{5/2} \rightarrow 4f_{7/2}\,(M_5)$ associated with the spin-orbit splitting. The relative intensities of the white lines were associated with the $4f$-shell occupancy of the rare-earth elements.[17–19] For cerium compounds, the white lines ratio in both EELS and XAS have been used to determine the valence of cerium ions.[20–22]

Figures 1(a) and 1(b) show the M_4 and M_5 edges of the EELS spectra of micron-size CeO_2 and $Ce_2(WO_4)_3$ particles, respectively. The valences of Ce ions in micron-size CeO_2 and $Ce_2(WO_4)_3$ are nominally 4^+ and 3^+, respectively. The intensity of the M_4 edge is higher than that of M_5 edge in Ce^{4+}, and reversed in Ce^{3+}. A number of methods have been developed to measure the M_5/M_4 ratio.[18,23,24] In this work, we chose the second derivative method to determine the white line ratio for our spectra, since it is insensitive to thickness variations.[25] The M_5/M_4 ratio is then determined by measuring the intensity of the M_5 and M_4 peaks in the second derivative of the spectra. Because of noise in the spectra, the raw data of the spectra must be smoothed to eliminate the channel-to-channel fluctuations. Here, we calculate the second derivative spectra from the acquired spectra based on the Savitzky-Golay method,[26] in which, for each point f_i, we least-squares fit a polynomial (m^{th} order) to all n_L+n_R+1 points in the moving window (n_L, n_R are the number of points to the left and right, respectively), and then set the second derivative g_i to be the value of the second derivative of that polynomial at position *i*. The advantage of using the Savitzky-Golay method over the moving window averaging method (e.g., used in the EL/P program) is that it provides smoothing without loss of resolution. Figures 1(c) and 1(d) show the second derivative spectra of the spectrum (a) and (b), respectively, with $n_L=n_R=32$ and $m=5$ (hereafter, we will use the same n_L, n_R and m for the all second derivative spectra). The M_5/M_4 ratio was then determined by measuring the maximum amplitude at the M_5 and M_4 peak in the second derivative. The M_5/M_4 ratios were 0.91 for Ce^{4+} and 1.31 for Ce^{3+} from these "standard" large particles. These ratios were determined from averaging a number of measurements (~10) from each of the standard samples and the standard deviations in the ratios were 0.03 for both samples. Also, these values of the ratios were close to values reported by Fortner *et al.*[20] Hence we used this procedure for determining the fraction of Ce^{3+} and Ce^{4+} ions in the particles.

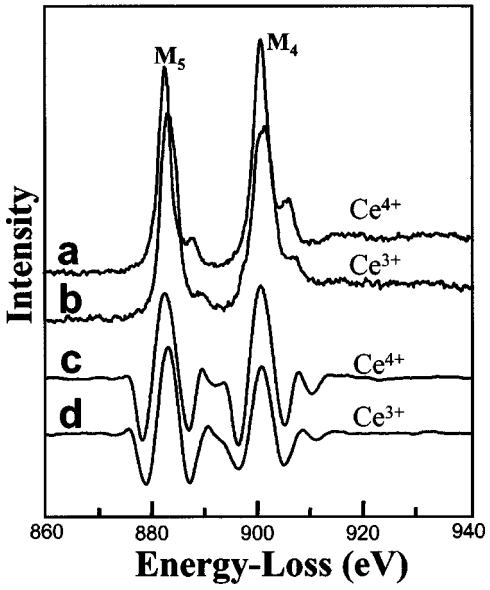

FIG. 1. EELS spectra of micron-size "standard" (a) CeO_2 and (b) $Ce_2(WO_4)_3$ particles. (c) Second derivative of (a) and (d) second derivative of (b).

III. EXPERIMENTAL RESULTS

Figures 2(a)–2(c) show examples of the high resolution images of CeO_{2-x} nanoparticles with different particle sizes

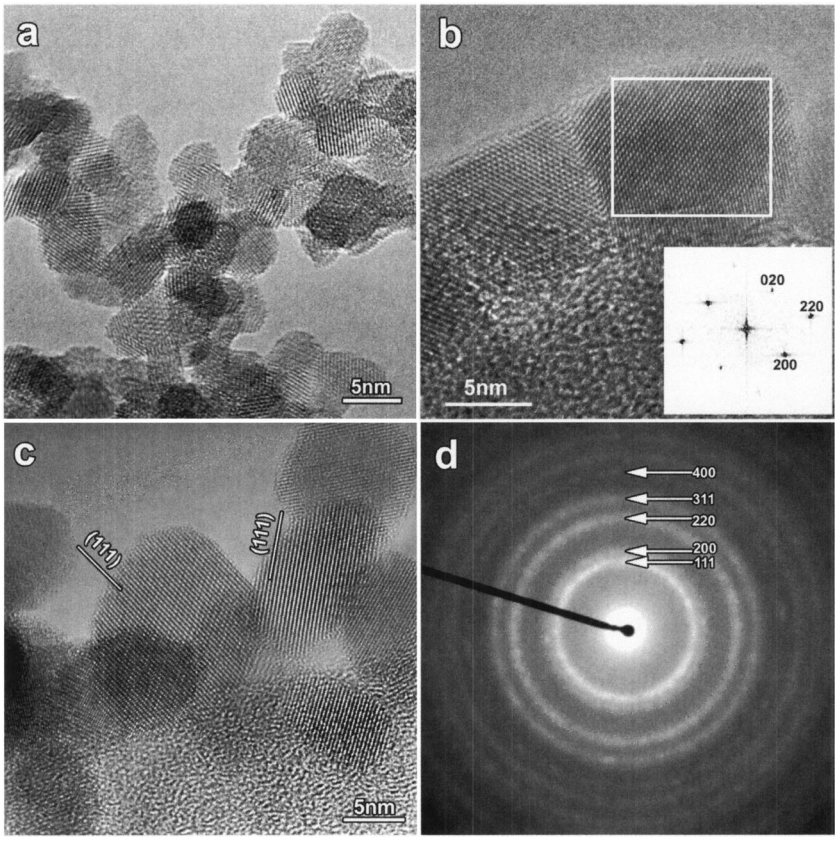

FIG. 2. (a)–(c) Examples of high resolution images of particles with different average size. The inset in (b) is the fast Fourier transform from the marked area. (d) Electron diffraction pattern from (a).

which were prepared in different helium atmospheres. Also shown in Fig. 2(d) is a selected-area electron diffraction pattern from the particles shown in Fig. 2(a). The particles were an agglomeration of single grains. The exact outlines of the particles varied, but were mostly circular or ellipsoidal, although there was some tendency toward forming squares with rounded corners for larger particles. Only on very rare occasions, did we observe particles with octahedral shape and surrounded by (111) planes, as reported by Zhang *et al.*[12] Although the (111) planes were clearly imaged in many of the particles shown in Fig. 2, these planes were not the terminating planes for the surfaces of these particles. As discussed below, this difference between the surface planes of the particles observed here and by Zhang *et al.*[12] is likely to be due to the difference in the preparation methods of the particles. These differences may result in different properties for these CeO_{2-x} nanoparticles.

The lattice parameter can be measured from the rings of a selected-area electron diffraction pattern from many particles. The lattice parameter measured by the rings is therefore the averaged value of many particles which in general have a range of particle sizes. To measure an individual particle, we use high resolution images. From a carefully calibrated high resolution image, we select the individual particle with its zone axis parallel to the beam direction and use a Fourier transform to get the diffractogram from that area, as shown in the inset of Fig. 2(b). The average lattice parameter of that individual particle is then measured from the spots in that diffractogram. Figure 3 shows the lattice parameters as a function of particle size measured with high resolution images. The data from Tsunekawa *et al.*[8,13] and Zhang *et al.*[12] are also shown in Fig. 3 for comparison. It is clear that the lattice parameter of CeO_{2-x} nanoparticles increases with decreasing particle size. The present particles show a larger lattice expansion than that reported by Tsunekawa *et al.*[8,13] and Zhang *et al.*[12] This is probably due to the non-

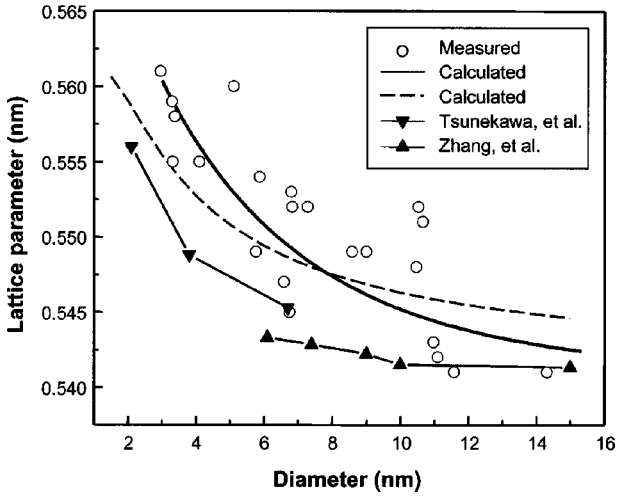

FIG. 3. Lattice parameter of CeO_{2-x} particles as a function of the particle size. The empty circles were measured from the high resolution images. The lattice parameters reported by Tsuenekawa *et al.* (Ref. 8) and Zhang *et al.* (Ref. 12) are also shown for comparison. Lattice parameters were calculated based on the micromechanical model described in the Appendix, and the solid and dashed lines are the calculations using the fitted Δd curve in Fig. 8 and $\Delta d = 0.561$ nm, respectively.

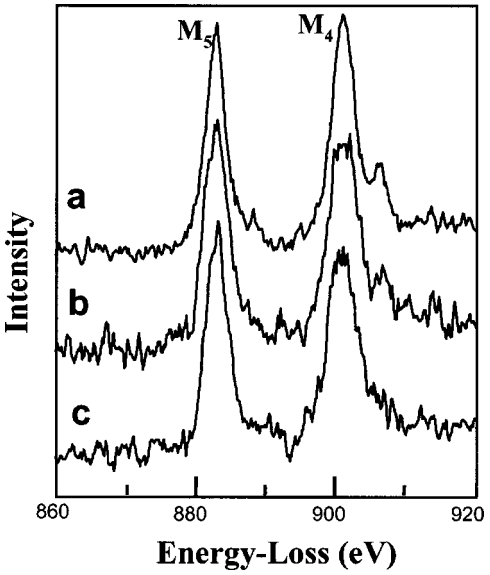

FIG. 4. EELS spectra from CeO_{2-x} nanoparticles with (a) $d=11$ nm, (b) $d=6$ nm, and (c) $d=3.5$ nm. The relative intensities of M_5 and M_4 in the spectra depend on the particle size.

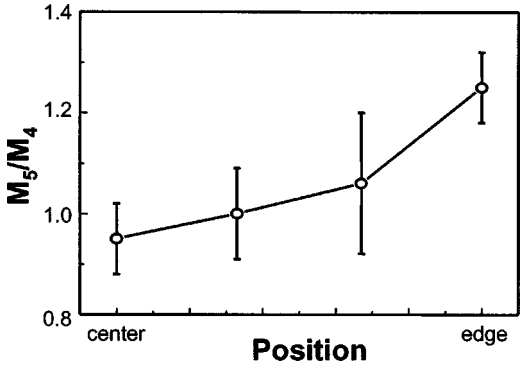

FIG. 6. M_5/M_4 ratios across the diameters of six CeO_{2-x} particles with diameters of approximately 13 nm. The distance between each point approximately 2 nm. Each point represents an average over the six particles, and the error bars show the statistical deviations for the six particles.

equilibrium particle formation process used in this study, as will be discussed in detail later.

EELS spectra from three particles with different sizes $d \cong 11$, 6, and 3.5 nm, are shown in Figs. 4(a)–4(c) qualitatively illustrating a systematic change in the EELS spectra with the particle size. Detailed analysis of the spectra indicates that the spectrum [Fig. 4(a)] from a particle with $d=11$ nm is close to that of Ce^{4+}, while that [Fig. 4(c)] for a 3.5 nm particle is close to that of Ce^{3+}. With the 0.13 nm probe size in our TEM, we explored the possible local variations in the Ce^{3+}/Ce^{4+} ratio in a given particle by selectively acquiring EELS spectrum from an edge (hence, the surface) and the central region for a given particle. This provides us an estimate of the volume fractions of cerium ions with 3^+ and 4^+ in the surface region and the interior of a particle. If, as shown in Fig. 5(a) (a sphere is shown for illustration purposes), the beam is focused at the center of a particle, the acquired EELS spectrum is primarily characteristic of the interior of the particle. However, if the beam is focused near the edge of the same particle [also Fig. 5(a)], the spectrum represents the surface region. Figure 5(b) shows an example of the spectrum variation as the electron beam was moved from the edge (less than 0.5 nm from the edge), to the center of a particle of ~15 nm in size. The spectrum from the center is close to that of Ce^{4+}, while that from the edge is close to Ce^{3+} as indicated by the M_5/M_4 ratios being 0.94 and 1.24 for the center and the edge, respectively. These correspond to the Ce^{3+} fraction of 7.5 and 83 %, respectively. A number of similar measurements were made from relatively large particles as well as around the perimeter of the particles, and essentially the same results as above were observed. This suggests that the valence reduction of cerium ions in a relatively large CeO_{2-x} nanopar-

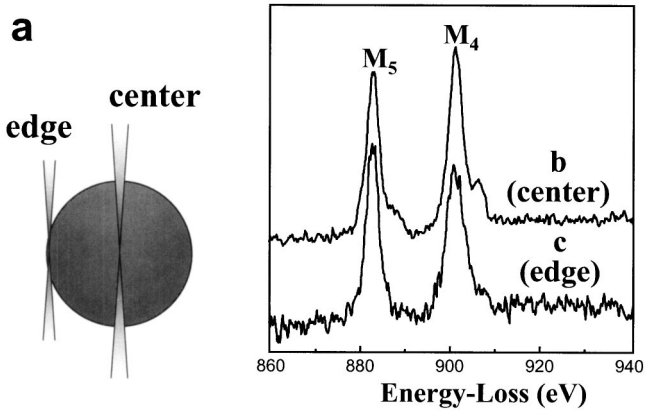

FIG. 5. (a) Experimental setup to measure the difference in the M_5/M_4 ratios between the surface and interior of a particle. The signal will mostly come from the surface when the beam is focused at the edge, while it will mainly come from the interior when the beam is focused at the center. EELS spectra obtained from the center (b) and edge (c) of a particle with $d=15$ nm.

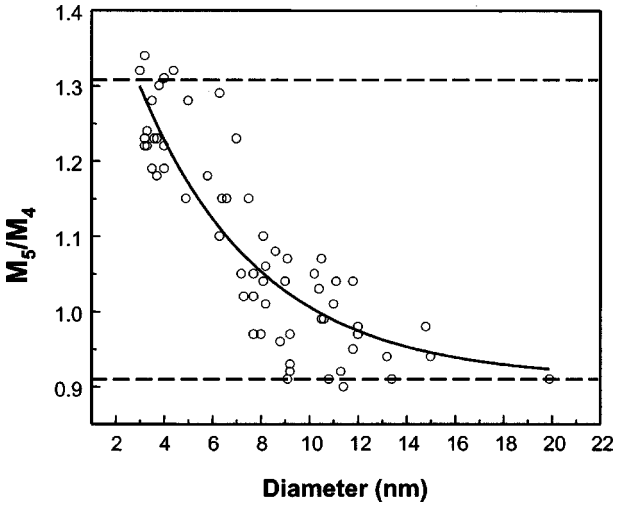

FIG. 7. Dependence of the M_5/M_4 ratios on the particle size of CeO_{2-x} nanoparticles. A fitted curve based on an exponential function is represented by the solid line.

ticles is primarily in the surface regions and not uniform throughout a particle.

In order to determine the extent of the reduced CeO_{2-x} surface layer, we have measured the M_5/M_4 ratios across the diameter of six CeO_{2-x} particles with approximate diameters of 13 nm. In order to avoid radiation damage, we have measured the ratios at four points from the center to the edge, and thus the distance between each point is approximately 2 nm and the results of the measurements are shown in Fig. 6. Considering the uncertainty in the precise position of the probe on each particle due to the specimen drift during the measurements, as well as the variations in the ratios from one particle to another of the same size, as shown below (Fig. 7), this result clearly confirms the above supposition about the reduction of Ce ions taking place primarily at or near the surface region, not uniformly across the particles. Also, the rapid drop in the M_5/M_4 ratio between the edge and the next interior point shows that the thickness of the reduced regions in relatively large particles is less than ~2 nm, but this could be a substantial overestimate of the thickness since it is limited by the large separation between points due to the experimental constraints mentioned above. This is also consistent with a theoretical prediction that the interior oxygen vacancies are unstable and tend to migrate to the surface in CeO_{2-x}.[27] However, we cannot rule out the presence of small amounts of oxygen vacancies in the interior of the particles which were produced by the vapor condensation method, a nonequilibrium process.

In Fig. 7, quantitative measurements of M_5/M_4 ratio from the second derivative spectra are summarized and plotted against particle size. The solid line in the figure is the fitted curve using an exponential function $M_5/M_4 = A\exp(-Bd)+0.91$, where d is the diameter of the particle, A and B are constants, $A=0.71$ and $B=0.2$. Based on the nearly linear relationship between the M_5/M_4 ratio and the occupancy of the $4f$ level for the light lanthanides, the formal valence of cerium ions may be estimated using a linear interpolation between the M_5/M_4 value for Ce^{4+} (0.91) and Ce^{3+} (1.31).[18] When the particle size is less than ~3 nm, the M_5/M_4 ratio is close to 1.31, so the valence of cerium ions is 3^+ throughout the particle. For the particle larger than ~15 nm, the M_5/M_4 ratio is close to 0.91, thus the cerium ions' valence is 4^+ in large particles. These data were all obtained by focusing the electron beam at the center of the particle and thus, each M_5/M_4 value is the average value over the particle.

The scatter in the data is in part due to the irregular shape of the particles. But it likely also reflects a real variation in Ce^{3+}/Ce^{4+} among particles made by this nonequilibrium process. During the evaporation and the particle formation process, some particles may lose more oxygen than others even among the particles similar in size since the terminating surface planes are different. It is well known that the ease in the reduction of CeO_2 at the surface depends strongly on the types of the terminating planes since the stability of the CeO_2 surfaces depends on the structure of the surface planes.[27] However, in spite of variations in the M_5/M_4 ratio, the trend of the rapid increase in the M_5/M_4 ratio as particle size decrease is apparent.

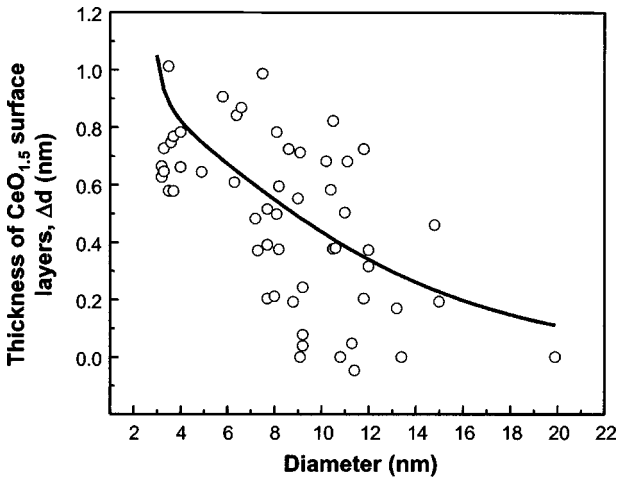

FIG. 8. The $CeO_{1.5}$ layer thickness as a function of particle size calculated from the M_5/M_4 ratio in Fig. 7 assuming all of Ce^{3+} are in the surface layer of each particle. The solid line was calculated from the fitted curve of Fig. 7.

IV. DISCUSSION

There are several aspects of the above observations on the nanocrystalline CeO_{2-x} particles which require some discussion. We first estimate the thickness and the volume fraction of $CeO_{1.5}$ layer from the experimentally determined M_5/M_4 ratios and compare them with those of previous studies. Then using a micromechanical model, we theoretically calculate the expected lattice parameters (averaged over the entire particle) of CeO_{2-x} particles with a nonuniform distribution of oxygen vacancies (as suggested by Fig. 6) which we approximate by a shell of $CeO_{1.5}$ covering the CeO_2 core as a function of particle size. While it is clear that such a core/shell spatial distribution of vacancies Ce^{3+} and Ce^{4+} ions is a crude approximation to the actual distribution, it is a reasonable first approximation to the segregation to the surface shown in Fig. 6. Such an approximation greatly simplifies the elasticity analysis, described in the Appendix, and the experimental information is too limited to constrain the parameters of a more elaborate model. The calculated and measured values of the lattice parameters, as well as those from previous works will then be compared. Finally, we discuss the possibility of the existence of the C-type sesquioxide structure for the smallest particles, which had been completely reduced to $CeO_{1.5}$.

Assuming that each particle consists of a thin surface layer of $CeO_{1.5}$ and a core of CeO_2, one can calculate the thickness Δd and the volume fraction f_v of $CeO_{1.5}$ layer for each particle from the M_5/M_4 ratio data. We first calculate Δd from a relationship $\Delta d = 0.5d[1-(1-f_b)^{1/3}]$. Here, d is the diameter of a sphere or the side of a cube, and we assume that the convergent incident beam (convergent angle ~11 mrad) was focused at the center of particle and that all of the Ce^{3+} ions existed in the form of $CeO_{1.5}$ at the surfaces; f_b is the fraction of Ce^{3+} in the volume which the electron beam passed through $f_b=(M_5/M_4-0.91)/(1.31-0.91)$. Then, we can calculate the volume fraction by $f_v = CeO_{1.5}/(CeO_{1.5}$

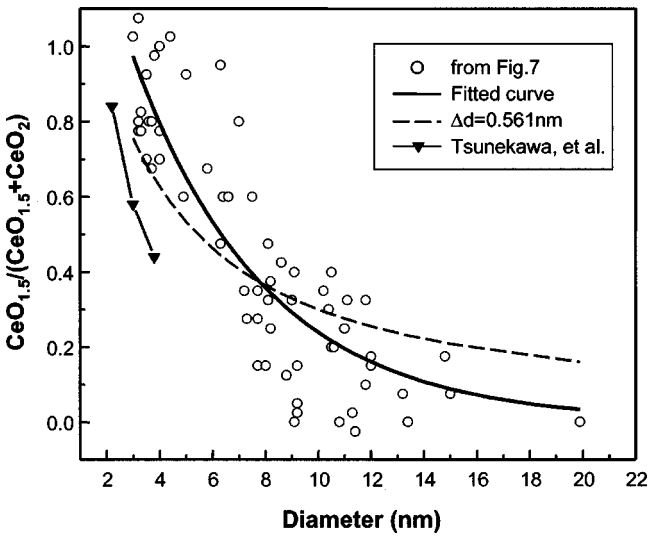

FIG. 9. The calculated $CeO_{1.5}/(CeO_2+CeO_{1.5})$ volume fraction as a function of particle size of CeO_{2-x} nanoparticles assuming all of the Ce^{3+} is in the thin surface layer of each particle. The solid line was calculated from the fitted curve of Fig. 7. The dashed line was calculated assuming the thickness of $CeO_{1.5}$ layer was a constant, equal to 0.561 nm. The data from Tsunakawa *et al.* (Ref. 8) are also shown for comparison.

$+CeO_2)=[d^3-(d-2\Delta d)^3]/d^3=f_b$ for a sphere. The same functional dependence of f_v on d is also obtained for a cube. Using these expressions, the thickness of the $CeO_{1.5}$ surface layer Δd and the volume fraction f_v of Ce^{3+} were calculated from the M_5/M_4 ratios shown in Fig. 7, and they are plotted as a function of the particle size in Figs. 8 and 9, respectively. The calculated Δd and f_v based on the fitted line in Fig. 7 are also shown as the solid lines in Figs. 8 and 9. As shown in Fig. 8, the thickness of the assumed $CeO_{1.5}$ layer is not constant with the particle size, but rapidly increases with decreasing size of the particles. This suggests that the increased volume fraction of $CeO_{1.5}$ is not due to the decreased size of the particles with a constant $CeO_{1.5}$ layer, but due to the increasingly larger losses of oxygen in smaller particles. As shown in Fig. 9, the volume fraction of $CeO_{1.5}$ also increases very rapidly for decreasing particle size, and the particles are practically fully reduced to $CeO_{1.5}$ for the particles below ~3 nm. For comparison purposes, the calculated volume fractions for the particles with a constant $CeO_{1.5}$ layer thickness of 0.561 nm are included as a dashed line in Fig. 9. Again it clearly illustrates that the increased volume fraction is not due to the shrinkage of the particles having a constant thickness of $CeO_{1.5}$ on surface for these particles which were processed by a vapor phase condensation. This result is also very surprising in comparison with the volume fractions which were reported by Tsunekawa *et al.*[5] and Zhang *et al.*[12] The former observed that the volume fractions of $CeO_{1.5}$ in CeO_{2-x} particles were 0.84, 0.58, and 0.44 for the particle size of 2.2, 3.0, and 3.8 nm, respectively (their data are included in Fig. 9, also), while the latter reported that the fraction of Ce^{3+} was 0.094 for the particles with an average diameter of 6.1 nm assuming that the oxygen vacancies were distributed uniformly throughout their particles.[7] These large differences in the amount of Ce^{3+} ions in small CeO_{2-x} particles appear to be due to the large differences in processing conditions. Particularly, those particles made by Zhang *et al.*[12] were octahedral in shape with (111) planes as the terminating surfaces. It is well known that the (111) surface is the most stable plane against the formation of surface oxygen vacancies.[27,28] Hence, it is more difficult to form a $CeO_{1.5}$ layer on this type of the particles than those having different terminating planes. Also, it is interesting to note that even though the processes used by Zhang *et al.*[12] and Tsunekawa *et al.*[13] to make these powders were different, both were low temperature chemical precipitation methods. However, the rate of the lattice expansion with decreasing particle size was very different. Thus, it appears that the degree of the reduction of CeO_2 accompanying the decrease in size of the particles depends strongly on the exact method which was used to synthesize these particles. Unfortunately, Tsunekawa *et al.*[8] reported neither the shape nor the surface planes for their particles. Thus we are unable to determine whether the shape and the surface crystallographic planes of the particles were actually the sources of these differences. It is also interesting to note that Tschope *et al.*[3] reported that nonstoichiometric CeO_2 powder, which was made by the evaporation of Ce metal and subsequent oxidation, exhibited greater catalytic activity than similarly sized powder which was made by a chemical precipitation. This difference in the catalytic properties of these powders may possibly be due to the similar differences discussed above in shape and terminating planes of the particles which were made by two different methods.

We used a micromechanical model, as described in the Appendix, to calculate the expected lattice parameter as a function of particle diameter for CeO_{2-x} particles which are assumed to consist of a layer of $CeO_{1.5}$ on a core of CeO_2. We compared the results with our measurements as well as those reported in earlier studies.[5,12] The calculation of the average parameter of a particle was performed by calculating the elastic strain state resulting from coherently matching the interface of the $CeO_{1.5}$ shell and the CeO_2 core. The lattice parameters for fluorite structure CeO_2 and average fluorite structure $CeO_{1.5}$ were taken to be 0.541 and 0.561 nm, respectively. The lattice parameter for $CeO_{1.5}$ was approximated to be one half of that of the C-type sesquioxide Ce_2O_3 proposed by Tsunekawa *et al.*[8] The details of the calculation are given in the Appendix. The results of calculations are shown in Fig. 3 and compared with our experimental data from high resolution images and those reported by Tsunekawa *et al.*[8] and Zhang *et al.*[12] The calculation (solid line) based on the fitted Δd curve in Fig. 8 is in a good agreement with our measurements (empty circle), while that (dashed line) based on a $CeO_{1.5}$ layer with constant thickness ($\Delta d=0.561$ nm) is relatively close to the data reported by Tsunekawa *et al.*[8] On the other hand, the increases in the lattice parameters with decreasing particle size for those reported by Zhang *et al.* were significantly smaller than ours and that of Tsunekawa *et al.* This implies that the surfaces of their particles were barely reduced to $CeO_{1.5}$ and the small increase in their lattice parameters with decreasing particle size could be due primarily to vacancies in bulk of the particles as they suggested from their measurements of line

broadening of Raman lines with decreasing size.[7]

As mentioned above, Tsunekawa *et al.* also suggested that their particles would be fully reduced to $CeO_{1.5}$ at the particle size of ~1.5 nm and that its crystal structure would be that of a C-type sesquioxide Ce_2O_3.[8] Since Ce_2O_3 with this structure has not been produced in bulk, it is of interest to search for this phase in our particles. This sesquioxide is a cubic and composed of eight unit cells of CeO_2 with ordered oxygen vacancies, and its lattice parameter is twice that of CeO_2. If this structure exists, there will be extra diffraction rings in Fig. 2(d) and we should be able to see these superlattice lines if their intensities are sufficient. In order to check this possibility, we first calculated the electronic structure factors for this structure and found that the (121) planes would have a significant intensity, though it would still be weak compared with that for (222) planes which are equivalent to (111) planes of the CeO_2 structure. The ratio of the calculated intensities for the lines corresponding to these planes was 0.0067. Since our particles of 3–4 nm are essentially $CeO_{1.5}$ as discussed above and the intensity of the diffraction rings, which are recorded on an image plate, has a very large dynamic range, we would expect to be able to see the 121 line. However, we could not detect this line even when the diffraction ring patterns were overexposed. Thus, we concluded that the structure of these small fully reduced $CeO_{1.5}$ particles is essentially that of CeO_2 fluorite structure, with two disordered oxygen vacancies per cubic unit cell. In addition, one can estimate the lattice parameter of fully reduced CeO_{2-x} ($x=0.5$) from Fig. 2 of Ref. 6 by taking the ionic radius of Ce^{3+} to be 0.1143 nm. (Figure 2 of Ref. 6 exhibits the rate of lattice expansion of CeO_{2-x} caused by the substitution of Ce^{4+} by rare earth ions with different ionic radii.) Then one obtains a lattice parameter of ~0.556 nm for $CeO_{1.5}$, and this is very close to that measured for very small particles (<~3 nm) of CeO_{2-x} in Fig. 3. This fact also supports the above observation of no superlattice line in the electron diffraction patterns even for the fully reduced CeO_{2-x} particles.

At this point, we speculate on the formation process. We assume that CeO_2 molecules are primarily evaporated and these collide with themselves as well as with He atoms in He atmosphere to form CeO_{2-x} particles. Since we found that higher He pressures made larger particles, the larger number of collisions produces larger particles. When the particles are still small (a few nm in diameter) the surface-to-volume fractions are large, and in this highly nonequilibrium process the surfaces of these particles will not likely be the most stable crystallographic planes, such as (111). Thus, the oxygen from CeO_2 is easily lost into an inert gas environment. When the particles grow in size, the oxygen vacancies in bulk or core of the particles are known to be unstable and tend to migrate to the surface.[27] Also, during the growth of large particles, there are likely to be more opportunities to develop stable surface planes, thus limiting the reduction of CeO_2 to only a very thin layer on the surface. In the middle of the range of the particle size which we studied, there were very large variations in both M_5/M_4 ratios and lattice parameter and thus, $CeO_{1.5}$ fractions. There are likely two reasons for this. One is the fact that, in this size range, some of the particles may start to form more crystallographically stable CeO_2 surfaces in some portions of the surface, while others may still be surrounded by the surfaces which are easily reduced. This will result in large particle-to-particle differences in the measured Ce^{3+}/Ce^{4+}. The other is related to the fact that the electron beams only penetrate through selected surface (the top and the bottom) as mentioned earlier. If one or both of these consists of the stable surfaces, the measured M_5/M_4 ratios reflect less Ce^{3+} ions, while if these surfaces happen to be less stable, the results show more Ce^{3+} ions in a given particle.

V. SUMMARY

In summary, the $M_{4,5}$-edge EELS spectra and lattice parameter have been used to evaluate the valence of cerium ions in cerium oxide nanoparticles. The measurement of the ratio of M_5/M_4 peak areas clearly shows the valence reduction of cerium ions with decreasing particle size, which is mainly due to the change of cerium ions from Ce^{4+} to Ce^{3+} at the surface. The measured M_5/M_4 ratios as a function of the nanoparticle size of CeO_{2-x}, which were made by a vapor phase condensation method, were used to determine the fraction of $CeO_{1.5}$ in these particles. Here we assumed that Ce^{3+} ions and Ce^{4+} ions existed separately as $CeO_{1.5}$ on the surface and CeO_2 as a core in large particles, based on the EELS measurements at the edge and the center of the particles. It was found that the amount of $CeO_{1.5}$ rapidly increased below a particle size of ~15 nm, and the particles were fully reduced (>90%) to $CeO_{1.5}$ at a size of ~3 nm or smaller. These increases in the fraction of $CeO_{1.5}$ took place at a much greater size than those reported previously. Since the stability of the surfaces of CeO_2 particles against the reduction depends strongly on the types of the surface planes, this difference is thought to be due to the differences in the synthesis methods of the particles which results in differences in the shape and the types of the crystallographic planes terminating surfaces.

ACKNOWLEDGMENTS

This work was performed under auspices of the Division of Materials Sciences, Office of Science, U.S. Department of Energy under Contract No. DE-AC-02-98CH10886. It was also partially supported by the Laboratory Directed Research and Development Program of Brookhaven National Laboratory.

APPENDIX: ELASTIC STRAIN STATE IN CORE-SHELL STRUCTURED CeO_{2-x} NANOPARTICLES

In earlier investigations Tsunakawa *et al.*[8] and Zhang *et al.*[12] measured the average lattice parameter a_0 of CeO_{2-x} nanoparticles as a function of particle size. Tsunakawa *et al.* estimated the oxygen content of their particles using a Vegard's rule linear relation between lattice parameters and deviation from ideal stoichiometry. This analysis implies a uniform distribution of regions of $CeO_{1.5}$ dissolved in CeO_2. However, our results indicate nonuniform distributions of

Ce^{3+} and Ce^{4+} (with accompanying oxygen vacancies) which can be approximated as a core-shell structure with a thin $CeO_{1.5}$ shell and a CeO_2 core. While this discrete separation into two regions (core and shell) is clearly an approximation to the actual spatial distribution, which probably is a continuous variation of stoichiometry, the rapid change in stoichiometry near the particle edge shown in Fig. 6 suggests that a core-shell structure is a reasonable first approximation to the actual distributions, and it greatly simplifies the analysis. In this Appendix we use a micromechanical model based on linear elasticity to estimate the effect of such a structure on the average lattice constant as a function of the size of the nanoparticles, which for simplicity we assume to be spherical.

We take a uniform spherical particle of CeO_2 of radius R with lattice parameter a_0 as our reference state and use hypothetical cutting-transformation-rejoining operations, after the manner of Eshelby,[29] to estimate the elastic strains resulting from surface layer deoxygenation. (We ignore changes of lattice parameter due to the surface stresses of the free surface, which can be shown to be negligible compared to variations caused by the oxygen nonstoichiometry.) We imagine removing a hollow spherical shell of thickness h from the surface of the particle and changing its composition to $CeO_{1.5}$ by removing oxygen atoms uniformly from the shell, with an accompanying expansion of the lattice of $(\Delta a_0/a_0)_{\max}$. We then apply surface tractions to the spherical core of CeO_2 and hollow spherical shell of $CeO_{1.5}$ so that their respective outer and inner surfaces match, rejoin them at the interface, remove the surface tractions and allow elastic deformation to occur until the internal stresses are balanced. This is readily done using the elastic solutions for spheres and spherical shells with radial displacement fields.[30] The result is that the core of CeO_2 of radius $R_c=R-h$ is in a state of uniform expansion and the shell of thickness h is compressed relative to its stress-free state. The volumetric strain of each of the two regions, referred to the lattice parameter a_0 of CeO_2 is

$$\left(\frac{\Delta a_0}{a_0}\right)_{\text{core}}=\left(\frac{\Delta a_0}{a_0}\right)_{\max}\left\{\frac{(R^3-R_c^3)}{(R^3-R_c^3)+(K_{\text{core}}/K_{\text{shell}})[R_c^3+R^3(3K_{\text{shell}}/4\mu_{\text{shell}})]}\right\} \tag{A1}$$

and

$$\left(\frac{\Delta a_0}{a_0}\right)_{\text{shell}}=\left(\frac{\Delta a_0}{a_0}\right)_{\max}\left[1-\frac{R_c^3}{(K_{\text{shell}}/K_{\text{core}})(R^3-R_c^3)+R_c^3+R^3(3K_{\text{shell}}/4\mu_{\text{shell}})}\right], \tag{A2}$$

where K and μ are the bulk modulus and shear modulus, respectively.

The volume average of the shift of the lattice parameter of the monoparticle from that in bulk stoichiometric CeO_2 is then given by

$$\left\langle\frac{\Delta a_0}{a_0}\right\rangle=\frac{R_c^3}{R^3}\left(\frac{\Delta a_0}{a_0}\right)_{\text{core}}+\frac{(R^3-R_c^3)}{R^3}\left(\frac{\Delta a_0}{a_0}\right)_{\text{shell}}. \tag{A3}$$

To proceed further requires inserting values of the elastic constants and an explicit relation between the core size R_c (or equivalently, the shell thickness h) as a function of particle size $R=R_c+h$.

Experimental data for the elastic constants of CeO_2,[31] yield a value for the ratio 3 K/4μ of 1.6, and we assume that this ratio remains the same for the $CeO_{1.5}$ shell. We used an ionic model of bonding to develop semiempirical scaling relations based on ionic charge states and interatomic spacings which describes the cohesive properties (lattice energy, elastic moduli, surface energies) of a number of fluorite structure halides and oxides with a precision of better that 10%.[32] This scaling relation applied to CeO_2 and $CeO_{1.5}$ yields a value of the ratio $K_{\text{core}}/K_{\text{shell}}$ of 1.68. With these values of the parameters, Eqs. (A1)–(A3) yield

$$\frac{\langle\Delta a_0(R)\rangle}{(\Delta a_0)_{\max}}=\frac{3.7f}{4.4-0.7f}, \tag{A4}$$

where f is the fraction of Ce ions in the particle which are in the shell (3^+ state)

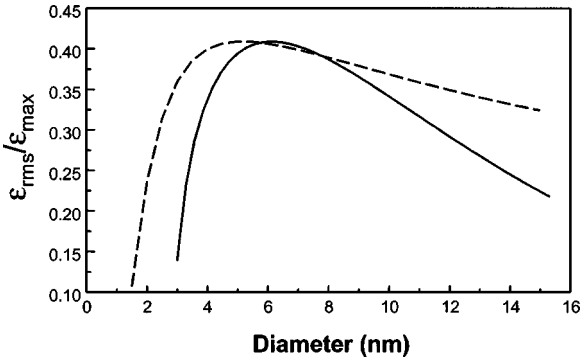

FIG. 10. The root-mean-square variations of the lattice parameters $\varepsilon\equiv\Delta a_0/a_0$ calculated using the micromechanical model described in the Appendix. The dashed line was obtained assuming a unit cell monolayer of $CeO_{1.5}$ on the surface, while the solid line was obtained with a $CeO_{1.5}$ layer thickness variation with particle size as shown in Fig. 8.

$$f = \frac{R^3 - (R-h)^3}{R^3}. \tag{A5}$$

These relations are used to calculate the lattice parameter as a function of radius for two different assumptions regarding the variation of shell thickness h with R: (1) the shell thickness is a constant value of one unit cell thickness, independent of R and (2) h varies with R as determined from the EELS data, shown in the fitted curve of Fig. 8.

The volume-averaged lattice parameter as a function of particle size computed with Eqs. (A4) and (A5), based on the two assumptions about $h(R)$, is shown in Fig. 3. The data of Tsunakawa *et al.*[8] and of Zhang *et al.*[12] are clearly seen to behave more as if there is a shell of constant thickness than as if h varies with size as shown by our data in Fig. 8.

In principle, measurements of x-ray diffraction line widths, corrected for particle size broadening, could be used to measure the inhomogeneity of the strain state produced by the core/shell structure of the nanoparticles. For completeness, we include here an expression for the mean square strain predicted by the micromechanical model

$$\frac{\langle \varepsilon^2 \rangle - \langle \varepsilon \rangle^2}{\varepsilon_{\max}^2} \equiv \left(\frac{\varepsilon_{\rm rms}}{\varepsilon_{\max}} \right)^2 = f(1-f) \times \left\{ \frac{(3K_{\rm shell}/4\mu_{\rm shell})}{1 + f[(K_{\rm shell}/K_{\rm core}) - 1] + 3K_{\rm shell}/4\mu_{\rm shell}} \right\}, \tag{A6}$$

where $\varepsilon \equiv \Delta a_0 / a_0$ and the angular brackets indicate a volume average. With the elastic parameters used above, this becomes

$$\left(\frac{\varepsilon_{\rm rms}}{\varepsilon_{\max}} \right)^2 = f(1-f) \left\{ \frac{1.6}{2.6 - 0.4f} \right\}. \tag{A7}$$

This is illustrated in Fig. 10 for the two assumptions above regarding the variation of shell thickness with particle size $h(R)$.

[1] For example see J. E. Kubsh, J. S. Rieck, and N. D. Spencer, *Catalysis and Automotive Pollution Control II* (Elsevier, Amsterdam, 1991).

[2] For example, see E. Perry Murray, T. Tsai, and S. A. Barnett, Nature (London) **400**, 649 (1999).

[3] A. Tschope, W. Liu, M. Flytzani-Stephanopoulos, and J. Y. Ying, J. Catal. **157**, 42 (1995).

[4] A. Tschope, D. Schaadt, R. Birringer, and J. Y. Ying, Nanostruct. Mater. **9**, 423 (1997).

[5] S. Tsunekawa, T. Fukuda, and A. Kasuya, Surf. Sci. **457**, L437 (2000).

[6] J. R. McBride, K. C. Hass, B. D. Poindexter, and W. H. Weber, J. Appl. Phys. **76**, 2435 (1994).

[7] J. E. Spanier, R. D. Robinson, F. Zhang, S.-W. Chan, and I. P. Herman, Phys. Rev. B **46**, 245407 (2001).

[8] S. Tsunekawa, R. Sivamohan, S. Ito, A. Kasuya, and T. Fukuda, Nanostruct. Mater. **11**, 141 (1999).

[9] Z. Wu, L. Guo, H. Li, Q. Yang, Q. Li, and H. Zhu, Mater. Sci. Eng., A **286**, 179 (2000).

[10] S. Tsunekawa, K. Ishikawa, Z.-Q. Li, Y. Kawazoe, and A. Kasuya, Phys. Rev. Lett. **85**, 3440 (2000).

[11] N. Guillou, L. C. Nistor, H. Fuess, and H. Hahn, Nanostruct. Mater. **8**, 545 (1997).

[12] F. Zhang, S.-W. Chan, J. E. Spanier, E. Apak, Q. Jin, R. D. Robinson, and I. R. Herman, Appl. Phys. Lett. **80**, 127 (2002).

[13] S. Tsunekawa, R. Sivamohan, T. Ohsuna, A. Kasuya, H. Takahashi, and K. Tohji, Mater. Sci. Forum **315–317**, 439 (1999).

[14] M. Hirano and E. Kato, J. Am. Ceram. Soc. **83**, 786 (1999).

[15] H. Baarnighausen and G. Schiller, J. Less-Common Met. **110**, 385 (1985).

[16] L. A. J. Garvie and P. R. Buseck, J. Phys. Chem. Solids **60**, 1943 (1999).

[17] B. T. Thole, G. van der Laan, J. C. Fuggle, G. A. Sawatzky, R. C. Karnatak, and J. M. Esteva, Phys. Rev. B **32**, 5107 (1985).

[18] T. Manoubi, C. Colliex, and P. Rez, J. Electron Spectrosc. Relat. Phenom. **50**, 1 (1990).

[19] G. Kaindl, G. Kalkowski, W. D. Brewer, B. Perscheid, and F. Holtzberg, J. Appl. Phys. **55**, 1910 (1984).

[20] J. A. Fortner, E. C. Buck, A. J. G. Ellison, and J. K. Bates, Ultramicroscopy **67**, 77 (1997).

[21] R. Niewa, Z. Hu, C. Grazioli, U. Robler, M. S. Golden, M. Knupfer, J. Fink, H. Giefers, G. Wortmann, F. M. F. de Groot, and F. J. DiSalvo, J. Alloys Compd. **346**, 129 (2002).

[22] F. F. Xu and Y. Bando, J. Appl. Phys. **89**, 5469 (2001).

[23] H. Kurata and C. Colliex, Phys. Rev. B **48**, 2102 (1993).

[24] D. H. Pearson, C. C. Ahn, and B. Fultz, Phys. Rev. B **47**, 8471 (1993).

[25] G. A. Botton, C. C. Appel, A. Horsewell, and W. M. Stobbs, J. Microsc. **180**, 122 (1995).

[26] W. H. Press, S. A. Teukolsky, W. T. Vetterling, and B. P. Flannery, *Numerical Recipes in C* (Press Syndicate of the University of Cambridge, Cambridge, 1992), p. 650.

[27] J. Conesa, Surf. Sci. **339**, 337 (1995).

[28] H. Cordatos, D. Ford, and R. J. Goorte, J. Phys. Chem. **100**, 18128 (1996).

[29] J. D. Eshelby, in *Solid State Physics*, edited by F. Seitz and D. Turnbull (Academic Press, New York, 1956), Vol. 3, pp. 79–144.

[30] L. D. Landau and E. M. Lifshitz, *Theory of Elasticity*, Vol. 7 of *Course of Theoretical Physics*, 3rd Eng. ed. (Pergamon Press, Oxford, 1986), pp. 18–19.

[31] A. Nakajima, A. Yoshihara, and M. Ishigame, Phys. Rev. B **50**, 13 297 (1994).

[32] D. O. Welch (unpublished).